Title
The STEP61 interactome reveals subunit-specific AMPA receptor binding and synaptic regulation

Journal
Proceedings of the National Academy of Sciences of the United States of America, 116(16)

ISSN
0027-8424

Authors
Won, Sehoon
Incontro, Salvatore
Li, Yan
et al.

Publication Date
2019-04-16

DOI
10.1073/pnas.1900878116

Peer reviewed

The $STEP_{61}$ interactome reveals subunit-specific AMPA receptor binding and synaptic regulation

Sehoon Won[a], Salvatore Incontro[b], Yan Li[c], Roger A. Nicoll[b,d,1], and Katherine W. Roche[a,1]

[a]Receptor Biology Section, National Institute of Neurological Disorders and Stroke, National Institutes of Health, Bethesda, MD 20892; [b]Department of Cellular and Molecular Pharmacology, University of California, San Francisco, CA 94158; [c]Protein/Peptide Sequencing Facility, National Institute of Neurological Disorders and Stroke, National Institutes of Health, Bethesda, MD 20892; and [d]Department of Physiology, University of California, San Francisco, CA 94158

Contributed by Roger A. Nicoll, February 27, 2019 (sent for review January 16, 2019; reviewed by David S. Bredt and Lin Mei)

Striatal-enriched protein tyrosine phosphatase (STEP) is a brain-specific protein phosphatase that regulates a variety of synaptic proteins, including NMDA receptors (NAMDRs). To better understand STEP's effect on other receptors, we used mass spectrometry to identify the $STEP_{61}$ interactome. We identified a number of known interactors, but also ones including the GluA2 subunit of AMPA receptors (AMPARs). We show that $STEP_{61}$ binds to the C termini of GluA2 and GluA3 as well as endogenous AMPARs in hippocampus. The synaptic expression of GluA2 and GluA3 is increased in STEP-KO mouse brain, and STEP knockdown in hippocampal slices increases AMPAR-mediated synaptic currents. Interestingly, $STEP_{61}$ overexpression reduces the synaptic expression and synaptic currents of both AMPARs and NMDARs. Furthermore, $STEP_{61}$ regulation of synaptic AMPARs is mediated by lysosomal degradation. Thus, we report a comprehensive list of $STEP_{61}$ binding partners, including AMPARs, and reveal a central role for $STEP_{61}$ in differentially organizing synaptic AMPARs and NMDARs.

STEP | LC/MS/MS | AMPA receptor | dephosphorylation | lysosome

Glutamate receptors are crucial for many aspects of synaptic function in the mammalian central nervous system, such as mediating the majority of excitatory neuronal transmission and inducing many forms of synaptic plasticity (1–5). Ionotropic glutamate receptors are classified into three large families: NMDA receptors (NMDARs), kainate receptors, and AMPA receptors (AMPARs). NMDARs fulfill essential roles in neuronal development, synaptic plasticity, and learning and memory (6–8) and assemble as heterotetramers (GluN1, GluN2A–D, GluN3A/B), most often consisting of two GluN1 subunits and two GluN2 subunits. Functional AMPARs are homo- or heterotetramers composed of combinations of four subunits (GluA1–4) (9). AMPARs account for much of the moment-to-moment rapid synaptic communication. In the hippocampus, canonical long-term potentiation is induced by NMDAR activation and expressed by an increase in the density of synaptic AMPARs (10–12). In fact, mechanisms underlying dynamic changes in synaptic AMPARs have been studied extensively, including lateral diffusion, exocytosis, and endocytosis followed by degradation (13–15).

One key mechanism regulating synaptic expression of both AMPARs and NMDARs is receptor phosphorylation (16). Many studies have demonstrated that activity-dependent subunit-specific phosphorylation of NMDARs and AMPARs has profound effects on synaptic localization and channel function (17–19). The GluN2 subunits of NMDARs have long cytosolic tails, which contain many phosphorylated S/T or Y residues. In particular, the GluN2B subunit has several well-characterized phosphorylation sites that have a profound effect on NMDAR trafficking (20, 21). Two key phosphorylation events occur at the extreme C terminus of GluN2B and control surface and synaptic expression: (*i*) GluN2B Y1472 is phosphorylated by the Src family tyrosine kinase Fyn within an endocytic motif (22) and blocks internalization by inhibiting binding to clathrin adaptor proteins, and (*ii*) GluN2B S1480 is phosphorylated by casein kinase 2 within the PDZ domain in an activity-dependent manner and blocks binding to the PSD-95 family of proteins, therefore destabilizing receptor surface and synaptic expression (23). These phosphorylation events are inversely related, and the relevant kinases and phosphatases work in concert to define synaptic NMDAR expression.

Striatal-enriched protein tyrosine phosphatase [STEP; also known as protein tyrosine phosphatase nonreceptor type 5 (PTPN5)] is expressed in the cortex, hippocampus, and striatum of brain (24, 25). The STEP family of proteins contains several splice variants. All STEP splice variants ($STEP_{61}$, $STEP_{46}$, $STEP_{38}$, and $STEP_{20}$) are highly expressed in striatum. In contrast, the full-length gene product, $STEP_{61}$, is the only variant expressed in cortex and hippocampus (26–28). The brain-specific tyrosine phosphatase STEP has been implicated in neuronal diseases (29) and neuropsychiatric disorders caused by its dysregulation (30–34). Previous studies have shown that STEP binds to protein kinases such as Fyn, ERK1/2, and Pyk2, and these are regulated by STEP dephosphorylating their critical functional tyrosine residues (35–38). Importantly, STEP dephosphorylates GluN2B Y1472, allowing the AP-2 clathrin-associated adaptor protein complex to bind to GluN2B, thereby leading to internalization of GluN2B-containing NMDAR complexes (39–41). We recently reported that $STEP_{61}$ binds to PSD-95 and that PSD-95 triggers $STEP_{61}$'s ubiquitination and degradation. Thus, STEP negatively regulates NMDARs by enhancing AP-2 binding and internalization, but STEP is down-regulated by the NMDAR scaffolding

Significance

Striatal-enriched protein tyrosine phosphatase (STEP) regulates the trafficking and function of a variety of synaptic proteins, including receptors and protein kinases. In addition, STEP's expression and activity are altered in many neuropsychiatric disorders. Here, we isolate the $STEP_{61}$ interactome, which includes known interactors such as NMDA receptor (NMDAR) subunits, PSD-95, and Fyn kinase. In addition, we identified the AMPA receptor (AMPAR) GluA2 subunit as a binding protein. We show that $STEP_{61}$ binds to the C termini of GluA2 and GluA3, but not GluA1. Furthermore, we show that $STEP_{61}$ dephosphorylates GluA2, thereby regulating synaptic GluA2-containing AMPARs via endocytosis and lysosomal degradation. $STEP_{61}$ preferentially regulates synaptic AMPARs and extrasynaptic NMDARs, revealing a role for $STEP_{61}$ in defining activity-dependent glutamate receptor localization.

Author contributions: S.W., S.I., R.A.N., and K.W.R. designed research; S.W., S.I., and Y.L. performed research; S.W., S.I., Y.L., R.A.N., and K.W.R. analyzed data; and S.W., S.I., Y.L., R.A.N., and K.W.R. wrote the paper.

Reviewers: D.S.B., Johnson & Johnson; and L.M., Case Western Reserve University.

The authors declare no conflict of interest.

[1]To whom correspondence may be addressed. Email: roger.nicoll@ucsf.edu or rochek@ninds.nih.gov.

This article contains supporting information online at www.pnas.org/lookup/suppl/doi:10.1073/pnas.1900878116/-/DCSupplemental.

Published online April 1, 2019.

protein PSD-95. There are many studies on the mechanisms by which STEP regulates NMDAR trafficking; however, AMPAR regulation by STEP is poorly understood, and STEP is not thought to directly bind to AMPARs (27, 42).

In this study, we use mass spectrometry (MS) to identify $STEP_{61}$ binding proteins. We prepared lysates from cortex and hippocampus of adult mouse brain to exclude binding partners specific to the shorter striatum-specific STEP variants. We identified the $STEP_{61}$ interactome, which included many of the expected binding partners, such as GluN2B, GluN1, AP-2, PSD-95, and Fyn. Interestingly, we also identified the AMPAR subunit GluA2. Additional analyses reveal that $STEP_{61}$ directly binds to the C termini of GluA2 and GluA3, but not GluA1. We also found that $STEP_{61}$ binding to GluA2 is necessary for tyrosine dephosphorylation of GluA2. We investigated the effect of $STEP_{61}$ expression on endogenous AMPARs and observed that the synaptic expression of GluA2 and GluA3 is significantly increased in STEP-knockout (STEP-KO) brain, whereas only extrasynaptic NMDA receptors are increased by STEP deletion (28). STEP-KO lysates increased tyrosine phosphorylation of GluA2, consistent with AMPAR binding and dephosphorylation being key STEP targets, because tyrosine phosphorylation of GluA2 is critical for its endocytosis. Also, STEP knockdown in organotypic slice culture increases AMPAR-mediated synaptic currents, but not NMDAR-mediated synaptic currents. Conversely, the overexpression of $STEP_{61}$ decreases the synaptic expression of GluA2 and GluA3 via lysosomal degradation as well as AMPAR-mediated synaptic currents. Our findings show that $STEP_{61}$ differentially organizes synaptic AMPARs and NMDARs.

Results

Identification of the $STEP_{61}$ Interactome. To identify $STEP_{61}$ binding proteins, we performed coimmunoprecipitation (co-IP) assays with STEP antibody from crude synaptosomal (P2) fractions from cortex and hippocampus of adult mouse brain. We analyzed $STEP_{61}$ binding proteins using liquid chromatography tandem MS (LC/MS/MS) (Fig. 1 *A* and *B*). We specifically used cortex and hippocampus because we recently showed that $STEP_{61}$ is the only STEP splice variant expressed in cortex and hippocampus (27, 28). In contrast, all STEP splice variants are expressed in striatum. We analyzed co-IPs from STEP-KO brain as a control for nonspecific binding to STEP antibody or other nonspecific contamination. From WT mouse brain samples, we identified 315 candidate proteins from three independent experiments (*SI Appendix*, Fig. S1 and Table S1), which we categorize in Fig. 1*B*: (*i*) 30% cytoskeletal-associated proteins and motor proteins (e.g., α-actinin, DBN1, myosin-10, MAP2, Arp2/3 complex); (*ii*) 20% vesicle trafficking proteins (e.g., AP-2, Rab3a, SNX1, SNX4, NBEA); (*iii*) 16% kinases and phosphatases (e.g., Fyn, PKA, PP2A, PP1); (*iv*) 8% ion channels, receptors, and transporters (e.g., GluN2B, GluN1, GluA2, mGluR5); (*v*) 8% ATP synthase and ATPases (e.g., Na^+/K^+-transporting ATPase α-subunit); (*vi*) 7% scaffolding proteins (e.g., PSD-95, SynGAP, Kalirin, Shank);

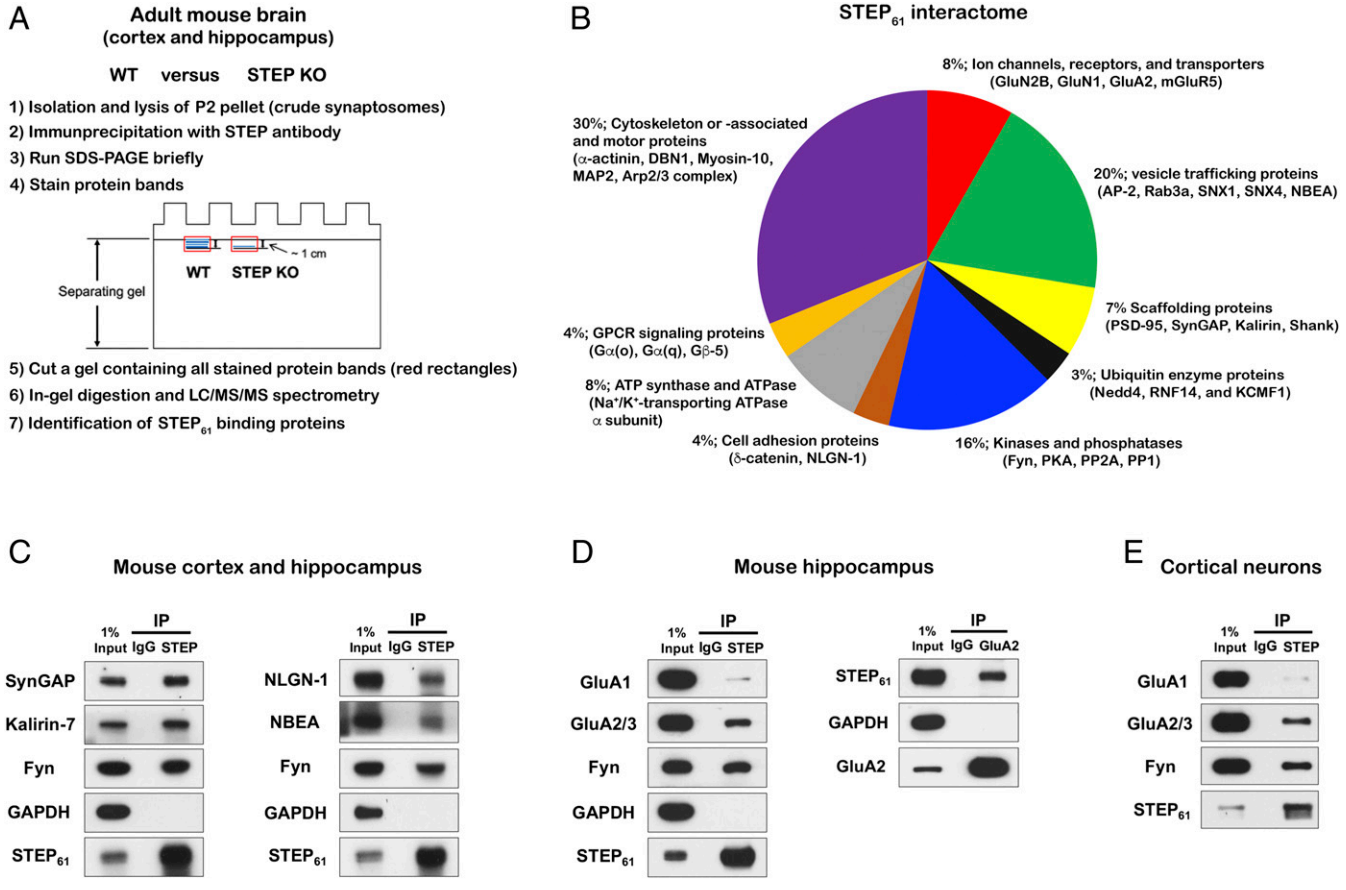

Fig. 1. $STEP_{61}$ binds to an extensive network of synaptic proteins, including AMPARs. (*A*) A descriptive drawing and strategy for LC/MS/MS analysis. After solubilization of P2 fraction from cortex and hippocampus of WT and STEP-KO adult mouse brain, binding proteins were immunoprecipitated with STEP antibody as described in *Materials and Methods* and identified. (*B*) Pie graph displays the categories of $STEP_{61}$ binding proteins. GPCR, G protein-coupled receptor. (*C*–*E*) P2 fractions of adult mouse cortex and hippocampus (*C*), adult mouse hippocampus (*D*), or primary cultured rat cortical neurons at DIV 21 (*E*) were solubilized with 1% sodium deoxycholate, neutralized with 1% Triton X-100 lysis buffer, and immunoprecipitated (IP) with STEP antibody or IgG as control or with GluA2 antibody, and then immunoblotted with indicated antibodies.

(*vii*) 4% cell adhesion proteins (e.g., δ-catenin, NLGN-1); (*viii*) 4% G protein-coupled receptor signaling proteins [e.g., Gα(o), Gα(q), Gβ-5]; and (*ix*) 3% ubiquitin enzyme proteins (e.g., Nedd4, RNF14, KCMF1). Among the proteins detected, we found PSD-95, which we recently demonstrated to be a $STEP_{61}$ interactor (28). We also detected the tyrosine kinase Fyn and NMDARs, which are well-known STEP binding proteins. Interestingly, we isolated E3 ubiquitin-protein ligases such as Nedd4, RNF14, and KCMF1, consistent with studies showing that $STEP_{61}$ is ubiquitinated (28, 43).

To evaluate the binding of $STEP_{61}$ protein to candidates from MS data, we selected scaffolding proteins (SynGAP, Kalirin-7), a cell adhesion protein (NLGN-1), and a vesicle trafficking protein (NBEA) and performed co-IP experiments using STEP antibody incubated with P2 fractions from adult mouse cortex and hippocampus (Fig. 1*C*). We confirmed that SynGAP, Kalirin-7, NLGN-1, and NBEA bind to $STEP_{61}$. Fyn was used as a positive control, and GAPDH as a negative control, for the co-IP experiments (28, 35). Among these $STEP_{61}$ binding proteins, we were specifically interested in the AMPAR subunit GluA2 (*SI Appendix*, Fig. S2) because it was an unexpected $STEP_{61}$ binding protein. To directly evaluate the binding of endogenous $STEP_{61}$ to endogenous AMPARs, we performed co-IP assays using STEP antibody incubated with P2 fractions from adult mouse hippocampus (Fig. 1*D*) or from lysates prepared from cultured cortical neurons at 28 days in vitro (DIV 28) (Fig. 1*E*). Immunoblotting for AMPARs revealed that the GluA2/3 subunits bind to $STEP_{61}$ robustly, whereas there was minimal GluA1 subunit detected. More specifically, when we immunoprecipitated endogenous GluA2 and immunoblotted for $STEP_{61}$, we found that $STEP_{61}$ binds to GluA2 in hippocampus (Fig. 1*D*).

The GluA2 C Terminus Binds to $STEP_{61}$ via the Kinase-Interacting Motif and Kinase-Specificity Sequence Domains, and $STEP_{61}$ Binding Is Necessary for Tyrosine Dephosphorylation of GluA2. To test whether all hippocampal AMPA receptors were competent to bind to STEP, we performed GST pull-down assays using GST-fused C-terminal domains of GluA1–3 incubated with lysates of $STEP_{61}$ expressed in HEK293T cells (Fig. 2 *A* and *B*). Interestingly, we found that $STEP_{61}$ binds to the C-terminal region of GluA2 and GluA3, but not GluA1 (Fig. 2*B*). As shown in Fig. 2*A*, GluA2 and GluA3 have tyrosine residues within the second half of the intracellular C-terminal domain, in contrast to GluA1. This result suggests that the tyrosine residues might be important targets for $STEP_{61}$. A previous study (44) showed that the Y876 residue on GluA2 is phosphorylated by Src family kinases. We tested whether the GST-GluA2-Y876A phospho-dead mutant affects the binding to $STEP_{61}$ using a GST pull-down assay and found that the Y876A mutant decreases its binding by 52% (Fig. 2*C*).

To delineate the binding region that mediates $STEP_{61}$ binding to GluA2, we used various $STEP_{61}$ deletion mutants (Fig. 2 *D* and *E*). We transfected $STEP_{61}$ mutant plasmids into HEK293T cells and performed pull-down assays using GST-GluA2 C-terminal fusion proteins and the lysates of expressed $STEP_{61}$ (WT or mutants). The middle region of $STEP_{61}$, including the kinase-interacting motif (KIM) and kinase-specificity sequence (KIS) domains (45), is important for its binding to the GluA2 C-terminal region (Fig. 2*D*). To confirm the relevance of each domain, we tested whether the KIM or KIS domain is important for GluA2 binding. Deletion of the KIS domain (ΔKIS-C) on $STEP_{61}$ decreased GluA2 binding by 45%, and the $STEP_{61}$ mutant (N), further deleted to omit the KIM domain, reduced the GluA2 binding to 7%. Thus, we reveal that the KIS domain affects GluA2 binding and the KIM domain is critical for the binding (Fig. 2*E*).

Next, we investigated whether $STEP_{61}$ binding to GluA2 regulates the dephosphorylation of GluA2 (Fig. 2*F*). We transfected $STEP_{61}$ and a deletion mutant (including the PTP domain only), which cannot bind to GluA2 but contains tyrosine phosphatase activity, with GluA2 and Fyn plasmids into HEK293T cells and immunoprecipitated with GluA2 antibody. We next performed immunoblotting with a pan phospho-tyrosine (pY) antibody (4G10) to detect pY-GluA2. We found that the $STEP_{61}$ deletion mutant (including the PTP domain only) does not dephosphorylate GluA2. This result shows that $STEP_{61}$ binding to GluA2 is necessary for dephosphorylation of GluA2.

AMPARs and NMDARs Are Differentially Regulated in STEP-KO Mouse Brain. To investigate whether $STEP_{61}$ can affect the expression of AMPARs and NMDARs in neurons, we performed a brain subcellular fractionation assay using WT and STEP-KO mouse brain (Fig. 3*A*). In the case of NMDAR subunits, the expression of GluN2A, GluN2B, and GluN1 is increased in total homogenate but is unchanged in the postsynaptic density (PSD) fraction (Fig. 3 *B* and *C*). This result is consistent with our previous study showing that STEP knockdown increases extrasynaptic NMDAR expression, whereas the expression of synaptic NMDAR subunits is not changed (28). In total homogenate of STEP-KO mouse brain, GluA2 expression is decreased, but GluA3 expression is increased (Fig. 3*B*). Interestingly, GluA2 and GluA3 are both significantly increased in the PSD fraction of STEP-KO mouse brain, whereas GluA1, PSD-95, and SAP102 are not changed in any fraction (Fig. 3 and *SI Appendix*, Fig. S3). Together, these data show that $STEP_{61}$ differentially regulates synaptic AMPARs and NMDARs.

In the case of GluA2, Src family tyrosine kinases phosphorylate its C-terminal domain and regulate its surface expression (44). To investigate whether $STEP_{61}$ regulates tyrosine phosphorylation of GluA2 at synapses, we performed a co-IP assay using a pan pY-antibody (4G10) with PSD fractions from WT or STEP-KO mouse brain. Immunoblotting for synaptic GluA2 showed that its tyrosine phosphorylation level is significantly increased in STEP-KO brain (Fig. 3*D*). Therefore, we demonstrated that STEP regulates the tyrosine phosphorylation level of synaptic GluA2, consistent with STEP stabilizing synaptic AMPAR.

STEP Knockdown Differentially Affects Whole-Cell and Synaptic AMPAR-Mediated Currents. To analyze the effects of STEP knockdown on the functional distribution of surface AMPARs, we performed electrophysiology in hippocampal organotypic slice culture (Fig. 4 *A* and *B*). We first coated gold nanoparticles with a STEP shRNA GFP-tagged plasmid. These particles were biolistically delivered to hippocampal slice cultures, and recordings were made 7 d later from a transfected cell and simultaneously from a neighboring control cell. Evoked AMPAR excitatory postsynaptic currents (EPSCs) were significantly increased (two- to threefold) in transfected neurons (Fig. 4 *C* and *D*). We used paired-pulse ratio as a measure of presynaptic contribution and found no significant change in the transfected neurons compared with control, confirming that the effect we observed is specifically postsynaptic (Fig. 4*E*). To measure surface AMPARs, picoliters of glutamate were puffed onto the patched dual cells through a large-diameter pipette. Intriguingly, AMPAR currents were significantly decreased in transfected neurons compared with control (Fig. 4 *F* and *G*).

$STEP_{61}$ Overexpression Regulates the Expression of Synaptic AMPARs and NMDARs. To examine whether $STEP_{61}$ overexpression affects the expression of total or synaptic AMPARs and NMDARs, we generated lentivirus expressing $STEP_{61}$, transduced cultured cortical neurons at DIV 17, and isolated total protein lysate at 7 d after transduction. The expression of the AMPAR subunits GluA1–3; NMDAR subunits GluN2A, GluN2B, and GluN1; and Fyn was not significantly changed in total lysate (Fig. 5*A*). Next, we performed a subcellular fractionation assay to isolate the PSD fraction from cultured cortical neurons after transduction with lentivirus expressing $STEP_{61}$. Interestingly, in addition to GluA2/3, the NMDAR subunits (GluN2A, GluN2B, and GluN1)

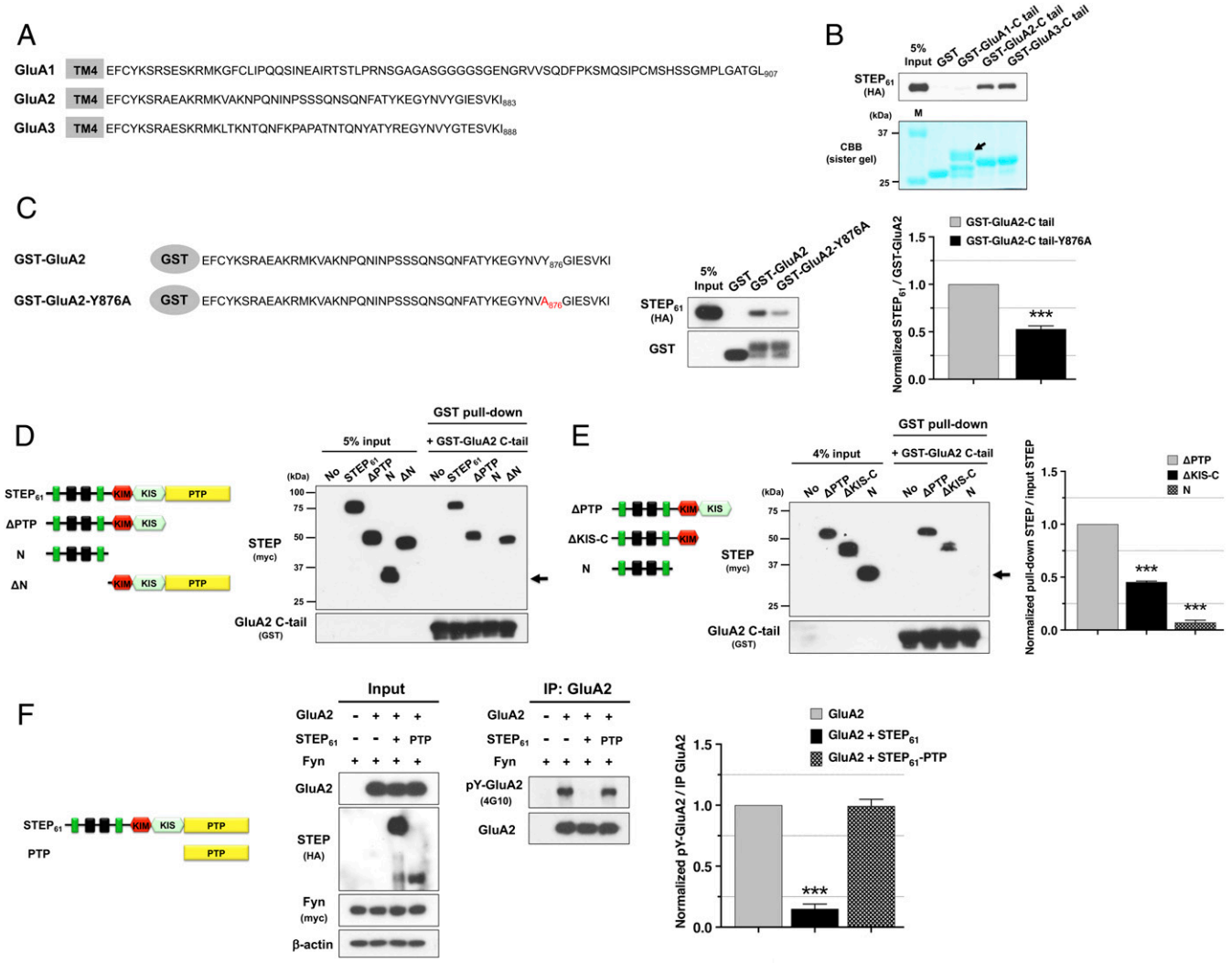

Fig. 2. Binding specificity for the AMPAR and $STEP_{61}$ interaction. (*A* and *C*) Amino acid sequence alignments of the GluA1–3 C termini (*A*) or the GST fusion proteins of wild type and the Y876A mutant of GluA2 C terminus (*C*). TM4 represents transmembrane 4. (*B*) GST alone or GST fusion proteins of the C termini of GluA1–3 or GluA2-Y876A were purified and used in a pull-down assay using the lysate of HA-tagged $STEP_{61}$ expressed in HEK293T cells. $STEP_{61}$ was detected with HA antibody. M indicates molecular weight marker; arrow indicates GST GluA1 C-terminal fusion protein. Quantification of blots normalized to each GST fusion protein ($n = 4$ independent experiments). GST-GluA2-C tail-Y876A ($P = 3.78e\text{-}06$). Error bars represent +SEM, $^{***}P < 0.001$. (*D* and *E*) Myc-tagged $STEP_{61}$ containing deletion mutants was expressed in HEK293T cells, and lysates were incubated with GST-GluA2 C terminus. After a pull-down assay, immunoblotting with myc antibody was performed. Arrows indicate the mutant protein of $STEP_{61}$. (*E, Right*) Quantification of GST pull-down blot normalized to each input STEP protein ($n = 3$ independent experiments). Deletion of the KIS domain (ΔKIS-C) ($P = 2.47e\text{-}07$) and the $STEP_{61}$ mutant (N) ($P = 8.75e\text{-}07$). Error bars represent +SEM, $^{***}P < 0.001$. (*F*) After the HA-tagged $STEP_{61}$ or deletion mutant (including PTP domain only) was expressed with Fyn and with FLAG-tagged GluA2 in HEK293T cells, the lysates were immunoprecipitated (IP) with GluA2 antibody, and then blotting was performed with indicated antibodies. (*F, Right*) Quantification of pY-GluA2 blot normalized to immunoprecipitated GluA2 ($n = 3$ independent experiments). $STEP_{61}$ ($P = 0.0001$) and PTP ($P = 0.9921$). Error bars represent +SEM, $^{***}P < 0.001$. (*D–F, Left*) Domain structure of $STEP_{61}$: proline-rich domain (green), transmembrane domain (black), KIM domain (red), KIS domain (light green), and PTP domain (yellow).

were also decreased in the PSD fraction upon $STEP_{61}$ overexpression. In contrast, GluA1 and Fyn were not altered (Fig. 5*B*). These data show that $STEP_{61}$ overexpression in primary neurons regulates the synaptic expression of AMPARs and NMDARs in a subunit-specific manner.

To investigate the underlying mechanism of $STEP_{61}$ effects on synaptic AMPARs, we transduced lentivirus expressing $STEP_{61}$ in cultured cortical neurons at DIV 17 and, after 6 d, treated with chloroquine (a lysosomal degradation blocker) or MG-132 (a proteasomal degradation blocker). We then isolated proteins from the PSD fraction. Interestingly, chloroquine treatment rescues GluA2/3 levels to control amounts, whereas MG-132 does not increase GluA2/3 levels. In contrast, GluA1 is not significantly changed by $STEP_{61}$ overexpression and drug treatment. This result shows $STEP_{61}$ regulation of synaptic GluA2/3 is mediated by lysosomal protein degradation (Fig. 5*C*). Similarly, we performed immunostaining in hippocampal cultures for GluA2 and PSD-95, as a synaptic marker, upon $STEP_{61}$ overexpression. We measured the colocalization of GluA2 overlapping with PSD-95 under different treatment conditions. We found that $STEP_{61}$ overexpression decreases the colocalization of GluA2 with PSD-95, but chloroquine increases its colocalization to control levels. Thus, these data show that $STEP_{61}$ regulates GluA2 at synapses via the lysosomal degradation pathway (Fig. 5*D*).

$STEP_{61}$ Overexpression Decreases AMPAR- and NMDAR-Mediated Synaptic Currents. To understand the functional effect of $STEP_{61}$ overexpression on AMPAR and NMDAR currents, we performed

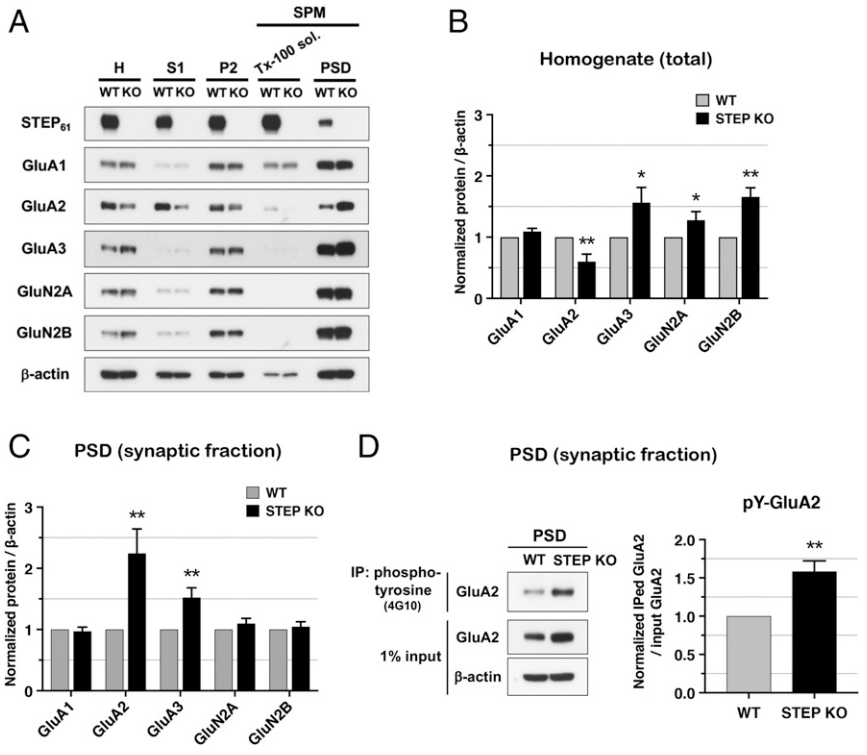

Fig. 3. AMPARs and NMDARs are differentially regulated in STEP-KO mouse brain. (*A*) Using adult WT and STEP-KO mouse forebrain, a subcellular fractionation assay was performed as described in *Materials and Methods*, and lysates were immunoblotted with indicated antibodies. H, homogenate; S1, supernatant; Tx-100 sol., soluble fraction. (*B–C*) Quantification of blots normalized to β-actin ($n = 5$ independent experiments). Each band intensity in homogenate (total) using GluA1 ($P = 0.066$), GluA2 ($P = 0.006$), GluA3 ($P = 0.026$), GluN2A ($P = 0.041$), and GluN2B ($P = 0.001$) (*B*), as well as GluA1 ($P = 0.339$), GluA2 ($P = 0.007$), GluA3 ($P = 0.006$), GluN2A ($P = 0.148$), and GluN2B ($P = 0.297$) in PSD (synaptic) fraction (*C*) was measured using ImageJ software. (*D*) The PSD fraction was isolated from WT and STEP-KO mouse brain, solubilized with 1% SDS lysis buffer, and neutralized with 1% Triton X-100 lysis buffer, and an immunoprecipitation (IP) assay was performed using 4G10 (pan pY) antibody. Proteins were resolved by SDS/PAGE and immunoblotted with GluA2 antibody. Quantification of blots normalized to input GluA2 ($n = 3$ independent experiments, $P = 0.007$). Error bars represent +SEM, $^*P < 0.05$, $^{**}P < 0.01$, P value is compared with WT.

electrophysiology in hippocampal organotypic slice culture (Fig. 6*A*). We biolistically delivered particles containing a plasmid encoding $STEP_{61}$. Slices were transfected at DIV 7, and recordings were conducted 2 to 3 d later. Evoked AMPAR and NMDAR EPSCs were significantly decreased in transfected neurons (Fig. 6 *B*, *C*, *F*, and *G*). In contrast, whole-cell AMPA and NMDA currents evoked by puffing glutamate in the presence of APV and NMDA/glycine, respectively, were unchanged (Fig. 6 *D*, *E*, *H*, and *I*). The fact that $STEP_{61}$ overexpression reduced synaptic currents, but not responses to agonist application, indicates that the effect of $STEP_{61}$ overexpression is specific for synaptic receptors.

Together, these data show that knockdown of STEP increases synaptic AMPAR-mediated currents. In addition, AMPAR synaptic expression is elevated in STEP-KO mouse brains, whereas STEP knockdown and STEP KO do not change synaptic NMDAR expression or currents. In contrast $STEP_{61}$ overexpression decreases synaptic currents for both AMPARs and NMDARs, demonstrating that $STEP_{61}$ differentially regulates the synaptic expression of glutamate receptors in a subunit-specific manner (Fig. 7).

Discussion

STEP is known to regulate synaptic function, and the up-regulation or down-regulation of STEP is implicated in a variety of neuropsychiatric disorders and excitotoxicity (29). In many cases, STEP protein levels are reported to be altered: They are increased in Alzheimer's disease, schizophrenia (31), and Fragile X syndrome and are decreased in Huntington's disease (46). For example, in Alzheimer's disease, amyloid beta (Aβ) binds to α7 nicotinic acetylcholine receptors, which activates PP2B/calcineurin and PP1 to dephosphorylate $STEP_{61}$, leading to an increase in $STEP_{61}$ protein levels (47). Aβ-induced inhibition of the ubiquitin proteasome system affects $STEP_{61}$ because it is a ubiquitinated protein (43). These studies suggest that the dysregulation of STEP protein levels is critical for neuropsychiatric disorders. Although STEP is known to regulate a variety of synaptic proteins, there has not been an unbiased characterization of STEP binding proteins. Therefore, we took the approach of using LC/MS/MS to identify $STEP_{61}$ binding proteins to define the $STEP_{61}$ interactome. STEP is known to be enriched in striatum, but the predominant full-length STEP splice variant, $STEP_{61}$, is also highly expressed in cortex and hippocampus. Therefore, we restricted our interactome screen to lysates from mouse cortex and hippocampus, and used STEP KO as a negative control. Using this approach, we identified 315 $STEP_{61}$ binding proteins. Some of these proteins were known interactors, such as GluN2B, GluN1, PSD-95, AP-2, and Fyn. However, we also found unexpected proteins, such as the AMPAR subunit GluA2; the vesicle trafficking proteins SNX1, SNX4, and NBEA; the scaffolding proteins SynGAP, Kalirin, and Shank; and the synapse adhesion molecule NLGN-1.

STEP is an important regulator of synaptic protein phosphorylation and trafficking. In particular, STEP dephosphorylates both NMDARs and AMPARs (48). In the case of NMDARs, many of the precise mechanisms of STEP regulation have been elucidated: STEP binds to the GluN2B subunit and dephosphorylates Y1472 within an endocytic motif, thereby causing endocytosis of GluN2B-containing NMDARs. However, the regulation of AMPARs by STEP is less clear, and the identification of GluA2 as a protein interactor was unexpected. AMPARs had been predicted targets of STEP, but an early study reported that GluA2 and STEP do not interact by co-IP (27). Therefore, in our current study, we carefully and comprehensively characterized the direct binding of GluA2 and STEP using several different assays. We found that $STEP_{61}$ binds to GluA2/3 in mouse brain hippocampus and cultured cortical neurons, whereas there is only weak binding of GluA1 (Fig. 1). We also demonstrated that $STEP_{61}$ directly binds to the C-terminal domains of GluA2 and GluA3, but not GluA1, in pull-down assays (Fig. 2). Importantly, we examined synaptic fractions and observed significant increases in GluA2 and GluA3 in the PSD fractions of STEP-KO brains, demonstrating an effect in vivo (Fig. 3). Again, the synaptic effects were on GluA2/3, but not GluA1. Moreover, we found that STEP knockdown increases AMPAR-mediated evoked EPSCs (eEPSCs) but decreases AMPAR-mediated whole-cell currents in hippocampal slice culture, which

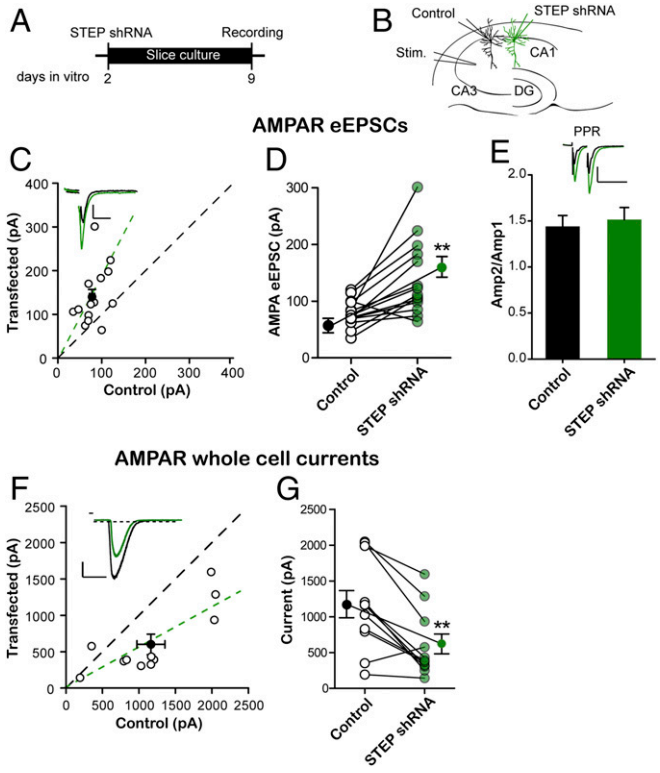

Fig. 4. STEP knockdown increases AMPAR EPSCs and decreases glutamate-elicited whole-cell currents. (*A*) Timeline of the experiment. (*B*) Scheme of the electrophysiological approach. (*C*) Scatterplot shows amplitudes of AMPAR EPSCs for single pairs (open circles) and mean ± SEM (filled circle) for STEP shRNA-transfected vs. control cells. (Scale bar: 50 ms, 50 pA.) (*D*) Paired average of single pairs from control and transfected cells. Means ± SEM for control and STEP shRNA are 78.56 ± 6.3 pA ($n = 15$) and 140.5 ± 17.8 pA ($n = 15$), respectively. $^{**}P = 0.0015$, Wilcoxon signed-rank test. (*E*) Paired-pulse ratio (PPR) traces and bar graph for control and transfected cells. Mean values of AMPAR second to first amplitude are 1.44 ± 0.1 ($n = 9$) and 1.5 ± 0.1 ($n = 9$), respectively. $P > 0.05$, Mann–Whitney *U* test. (Scale bar: 100 ms, 100 pA.) (*F*) Scatterplot showing whole-cell currents in response to fast application of glutamate in the presence of tetrodotoxin and APV, holding cells at −70 mV. Data represent pairs of simultaneously recorded neurons in slice cultures from STEP shRNA-transfected and neighboring control cells. (Scale bar: 5 s, 100 pA.) (*G*) Paired average of single pairs from control and transfected cells. Means ± SEM for control and STEP shRNA are 629.7 ± 131.2 pA ($n = 9$) and 640.4 ± 99.9 pA ($n = 9$), respectively. $^{**}P = 0.91$, Wilcoxon signed-rank test. DG, dentate gyrus; Stim., stimulus.

is consistent with the expression levels of GluA2 in STEP-KO mouse brain.

Previous studies have meticulously examined the subunit composition of AMPARs in hippocampus (49). GluA1/2 heteromers are the dominant AMPARs; about 80% of all synaptic AMPARs in CA1 hippocampal pyramidal cells are GluA1/2 heteromers, and more than 95% of extrasynaptic AMPARs are GluA1/2 heteromers. However, there is a smaller (∼15%) but significant population of GluA2/3 heteromers that are enriched at synapses in CA1 of hippocampal pyramidal cells. Clearly, GluA2-containing AMPAR complexes are dominant in hippocampus. In addition, the GluA2 subunit is critical for certain types of plasticity. Specifically, it is key to synaptic scaling, which is regulated by the GluA2 C-terminal domain (50). In other studies, STEP has been shown to be regulated during homeostatic plasticity. The changes in $STEP_{61}$ levels regulate the tyrosine phosphorylation of the C-terminal domain of GluA2 (48), suggesting that $STEP_{61}$ tyrosine dephosphorylation of GluA2 regulates the surface and synaptic expression of GluA2-containing AMPARs. In our study, we found that tyrosine phosphorylation of GluA2 in STEP-KO brains is significantly increased (Fig. 3*D*).

In our previous study (28), we showed that PSD-95 directly binds to $STEP_{61}$, leading to ubiquitination and degradation of $STEP_{61}$ in a proteasome-dependent manner. We also found that $STEP_{61}$ expression is increased by PSD-95 knockdown as well as in PSD-95–KO mouse brain (28). PSD-95 stabilizes synaptic NMDARs by direct binding, as well as by triggering the degradation of the negative regulator $STEP_{61}$. However, when we knock down STEP, extrasynaptic expression of NMDARs is increased, but synaptic expression of NMDARs is not changed (28). Similarly, GluN2B is not changed in the PSD fraction of STEP-KO neurons; however, the expression of NMDARs is increased in total homogenate. Thus, for NMDARs, PSD-95 strongly regulates synaptic receptors, whereas $STEP_{61}$ regulates extrasynaptic pools. Strikingly, STEP has a distinct effect on synaptic AMPARs. In the STEP KO, synaptic GluA2 and GluA3 are dramatically increased, but not GluA1 (Fig. 3). Thus, STEP robustly regulates both AMPARs and NMDARs, but with differential synaptic effects.

STEP has several splice variants, including $STEP_{61}$, $STEP_{46}$, $STEP_{38}$, and $STEP_{20}$, which are expressed in striatum, whereas only $STEP_{61}$ is expressed in cortex and hippocampus (24, 27, 28, 51, 52). The long form, $STEP_{61}$, is an integral membrane protein, whereas some of the shorter variants lack the transmembrane domains and are cytosolic (52). It is important to emphasize that $STEP_{61}$ interacts with PSD-95 through the N-terminal domain of $STEP_{61}$, which is not included in $STEP_{46}$. In our current study, we show that GluA2 and GluA3 interact with the KIM and KIS domains of $STEP_{61}$, which are also included in $STEP_{46}$. In previous studies, many groups purified and introduced $STEP_{46}$, the soluble variant of STEP, into cultured hippocampal and cortical neurons to examine the effect of STEP protein overexpression on NMDAR and AMPAR trafficking (27, 42, 48, 53, 54), even though only $STEP_{61}$ is expressed in mouse cortex and hippocampus. This soluble form would clearly disrupt some interactions, but not others, and the results should be interpreted with caution. In our studies, we have used lentivirus expressing full-length $STEP_{61}$ to investigate whether $STEP_{61}$ overexpression regulates the total and synaptic expression of AMPARs and NMDARs. Total protein levels of AMPARs and NMDARs are not significantly changed upon $STEP_{61}$ overexpression in cultured cortical neurons, whereas $STEP_{61}$ overexpression decreases synaptic GluA2, GluA3, and NMDAR subunits (GluN1, GluN2A, GluN2B), but not GluA1 or Fyn (Fig. 5). Interestingly, $STEP_{61}$ regulation of synaptic GluA2/3 is related to lysosomal degradation. Furthermore, using hippocampal slices, we found that $STEP_{61}$ overexpression does not change AMPAR and NMDAR whole-cell currents. Interestingly, AMPAR-mediated and NMDAR-mediated eEPSCs are remarkably decreased upon $STEP_{61}$ overexpression (Fig. 6). Thus, the overexpression of $STEP_{61}$ affected the synaptic expression of AMPARs and NMDARs, as well as AMPAR-mediated and NMDAR-mediated synaptic currents. Both AMPARs and NMDARs are trafficked in and out of synaptic regions and undergo endocytosis mediated by $STEP_{61}$ tyrosine dephosphorylation at steady state, thereby maintaining a balance of receptors. However, STEP KO or STEP knockdown increases synaptic AMPARs and extrasynaptic NMDARs, suggesting that synaptic NMDAR capacity is saturated at steady-state and the deletion of STEP preferentially accumulates extrasynaptic NMDARs. In sharp contrast, deletion of STEP increases synaptic AMPARs, consistent with a broader dynamic range for the density of AMPARs. In contrast, $STEP_{61}$ overexpression decreases both synaptic AMPARs and NMDARs, demonstrating that acute down-regulation of synaptic glutamate receptors by $STEP_{61}$ is conserved for AMPARs and NMDARs (Fig. 7). Overall, our data show that $STEP_{61}$ has differential subunit-specific effects on synaptic AMPARs compared with NMDARs.

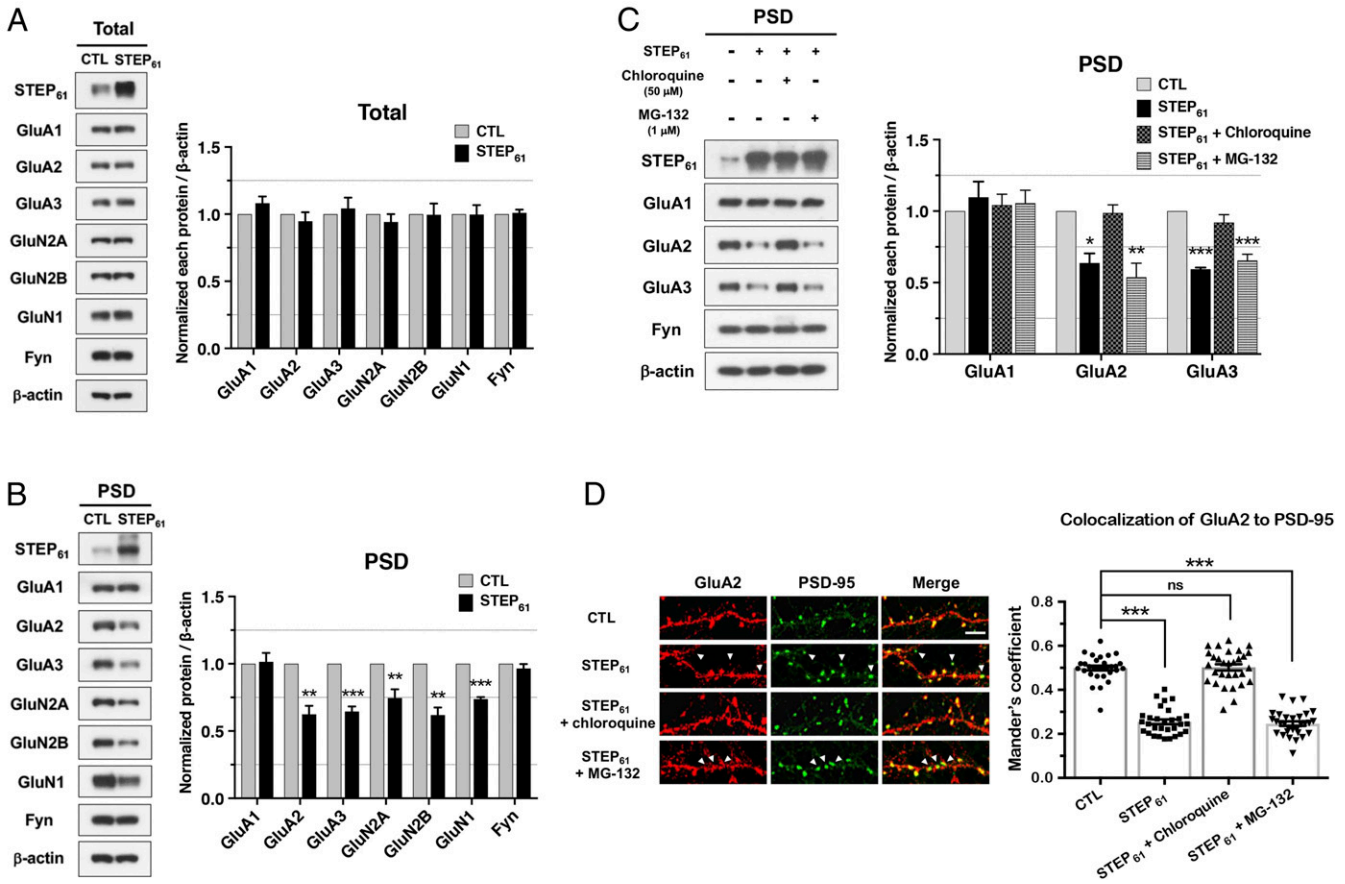

Fig. 5. $STEP_{61}$ overexpression regulates the synaptic expression of AMPARs and NMDARs, and $STEP_{61}$ regulation of synaptic AMPARs is through the lysosomal degradation pathway. (*A–C*) Primary cortical neurons were transduced with lentivirus expressing $STEP_{61}$ at DIV 17, and 7 d later, total protein lysate (n = 5 independent experiments) or PSD fraction (n = 3 independent experiments) was isolated and immunoblotted with GluA1 (P = 0.072), GluA2 (P = 0.227), GluA3 (P = 0.306), GluN2A (P = 0.172), GluN2B (P = 0.479), GluN1 (P = 0.483), and Fyn (P = 0.357) in total lysate (*A*), as well as with GluA1 (P = 0.421), GluA2 (P = 0.002), GluA3 (P = 3.628e-04), GluN2A (P = 0.009), GluN2B (P = 0.001), GluN1 (P = 3.077e-05), and Fyn (P = 0.173) in PSD fraction (*B*). (*C*) Chloroquine (50 μM) or MG-132 (1 μM) was applied for 18 h before protein isolation from the PSD fraction. Immunoblotting was performed (n = 3 independent experiments) with GluA1 ($STEP_{61}$, P = 0.7360; $STEP_{61}$ + chloroquine, P = 0.9645; and $STEP_{61}$ + MG-132, P = 0.9278), GluA2 ($STEP_{61}$, P = 0.0116; $STEP_{61}$ + chloroquine, P = 0.9979; and $STEP_{61}$ + MG-132, P = 0029), and GluA3 ($STEP_{61}$, P = 0.0001; $STEP_{61}$ + chloroquine, P = 0.3268; and $STEP_{61}$ + MG-132, P = 0.0004). All blots were normalized to β-actin. Dunnett's one-way ANOVA test was performed. Error bars represent +SEM, $*P < 0.05$, $**P < 0.01$, $***P < 0.001$, P value is compared with control (CTL). (*D, Left*) Primary hippocampal neurons were transfected with pCAG-IRES-mCherry or pCAG-$STEP_{61}$-IRES-mCherry at DIV 10 and immunostained at DIV 20. After fixation and permeabilization, total GluA2 was labeled with anti-GluA2 and Alexa 555-conjugated secondary antibody (red), and PSD-95 was visualized with anti-PSD-95 and Alexa 488-conjugated secondary antibody (green). (Scale bar: 5 μm.). Arrowheads indicate GluA2 nonoverlapping with PSD-95 puncta. (*D, Right*) $STEP_{61}$ (P = 0.0001), $STEP_{61}$ + chloroquine (P = 0.9953), and $STEP_{61}$ + MG-132 (P = 0.0001), Dunnett's one-way ANOVA test. Error bars represent ±SEM, $***P < 0.001$, P value is compared with CTL. ns, not significant.

Our current findings broaden our understanding of STEP and its functional influence on excitatory synapses. In particular, we demonstrate that $STEP_{61}$ directly binds to AMPARs, which had previously been reported not to be the case (27). Because it was unexpected, we evaluated this finding in a comprehensive manner using STEP knockdown and $STEP_{61}$ overexpression. In addition, we focused on STEP-KO brains to elucidate the changes in AMPAR and NMDAR expression in the PSD fraction in vivo. Overall, our results demonstrate that $STEP_{61}$ differentially regulates AMPAR and NMDAR trafficking. Although $STEP_{61}$ exerts its influence by dephosphorylating key tyrosines on the C termini of AMPARs and NMDARs, the synaptic effects are distinct. Our data reveal that $STEP_{61}$ acts as a master organizer of synaptic versus extrasynaptic glutamate receptors.

Materials and Methods

cDNA Constructs. Human $STEP_{61}$ (PTPN5) was subcloned with an N-terminal myc or HA tag (28). A truncation mutant of $STEP_{61}$ (ΔPTP, N, ΔKIS-C, ΔN, or PTP) was deleted 262 amino acids from Phe^{304}, deleted 369 amino acids from Met^{197}, deleted 312 amino acids from Cys^{254}, started with Met^{197} , or started with Phe^{304}, respectively. Rat GluA1–3 C termini were tagged with C-terminal GST, and each C terminus starts with Glu^{827} or Glu^{834} or Glu^{839}, respectively.

Antibodies. Mouse anti-STEP (cat. no. NB300-202; Novagen), rabbit anti-SynGAP (cat. no. 3200; Cell Signaling), rabbit anti–Kalirin-7 (laboratory made), mouse anti–NLGN-1 (cat. no. 129111; Synaptic Systems), rabbit anti-NBEA (cat. no. 194003; Synaptic Systems), rabbit anti-GluA1 (custom made), rabbit anti-GluA2/3 (55), mouse anti-GluA2 (clone L21/32; NeuroMab), rabbit anti-GluA2 (cat. 82103; Synaptic Systems), rabbit anti-GluA3 (cat. no. 3437; Cell Signaling), rabbit anti-GluN2A (cat. no. M264; Sigma), mouse anti-GluN2B (clone N59/36; NeuroMab), mouse anti-GluN1 (28), mouse anti–PSD-95 (clone K28/43; NeuroMab), mouse anti-SAP102 (clone N19/2; NeuroMab), rabbit anti-Fyn (cat. no. 4023; Cell Signaling), rabbit anti-Src (cat. no. 2110; Cell Signaling), mouse anti-GAPDH (cat. no. sc-365062; Santa Cruz), mouse anti-FLAG (cat. no. F1804; Sigma), rabbit anti-FLAG (cat. no. 7425; Sigma), rabbit anti-HA (cat. no. 3724; Cell Signaling), mouse anti-HA (cat. no. 2367; Cell Signaling), rabbit anti-myc (cat. no. 2278; Cell Signaling), rabbit anti-GST (cat. no. A190-122A; Bethyl Laboratories), mouse anti–β-actin (cat. no. G043; abm), and mouse anti-4G10 (cat. no. 05-321; Millipore).

LC/MS/MS Sample Treatment. After immunoprecipitation with STEP antibody, proteins were resolved by SDS/PAGE. Gel bands for each sample were excised,

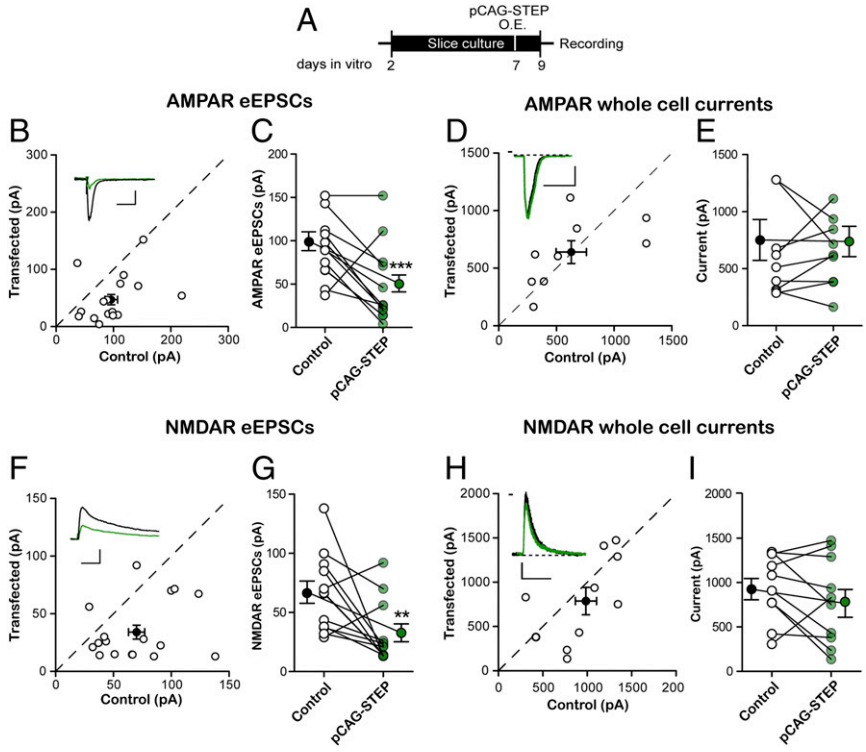

Fig. 6. $STEP_{61}$ overexpression (pCAG-STEP O.E.) decreases AMPAR and NMDAR EPSCs, but whole-cell currents do not change. (*A*) Timeline of the experiment. (*B*) Scatterplot shows amplitudes of AMPAR EPSCs for single pairs (open circles) and mean ± SEM (filled circle) for STEP O.E. transfected vs. control cells. (Scale bar: 50 ms, 50 pA.) (*C*) Paired average of single pairs from control and transfected cells. Means ± SEM for control and STEP O.E. (pCAG-STEP) are 96.41 ± 11 pA ($n = 17$) and 47.24 ± 9.8 pA ($n = 17$), respectively. ***$P = 0.004$, Wilcoxon signed-rank test. (*D*) Scatterplot showing whole-cell currents in response to fast application of glutamate in the presence of tetrodotoxin and APV, holding cells at −70 mV. Data represent pairs of simultaneously recorded neurons in slice cultures from transfected and neighboring control cells. (Scale bar: 5 s, 100 pA.) (*E*) Paired average of single pairs from control and transfected cells. Means ± SEM for control and STEP O.E. (pCAG-STEP) are 629.7 ± 131.2 pA ($n = 9$) and 640.4 ± 99.89 ($n = 9$), respectively. $P = 0.91$, Wilcoxon signed-rank test. (*F*) Scatterplot shows amplitudes of NMDAR EPSCs for single pairs (open circles) and mean ± SEM (filled circle) for STEP O.E. transfected vs. control cells. (Scale bar: 50 ms, 50 pA.) (*G*) Paired average of single pairs from control and transfected cells. Means ± SEM for control and STEP O.E. (pCAG-STEP) are 70 ± 7.97 pA ($n = 17$) and 34.65 ± 6.24 pA ($n = 17$), respectively. **$P = 0.002$, Wilcoxon signed-rank test. (*H*) Scatterplot showing whole-cell currents in response to fast application of NMDA. Data represent pairs of simultaneously recorded neurons in slice cultures from transfected and neighboring control cells. (Scale bar: 5 s, 100 pA.) (*I*) Paired average of single pairs from control and transfected cells. Means ± SEM for control and STEP O.E. (pCAG-STEP) are 946.6 ± 119.2 pA ($n = 10$) and 787.8 ± 155.1 pA ($n = 10$), respectively. $P = 0.27$, Wilcoxon signed-rank test.

cut, and washed. Proteins were digested without being reduced and alkylated. A 100-μL volume of freshly made trypsin (Promega) solution (5 ng/μL in 50 mM ammonium bicarbonate) was added to each sample. Trypsin digestion was performed overnight at 37 °C in an incubator. Tryptic peptides were extracted from the gel and desalted using an Oasis HLB μElution plate (Waters).

LC/MS/MS Analysis. An ES802 nanocolumn (Thermo Fisher Scientific) was used for the online peptide separation at a flow rate of 300 nL/min. Unless otherwise indicated, a 90-min data-dependent LC/MS/MS experiment was performed for each sample on a system in which an Orbitrap Elite mass spectrometer (Thermo Fisher Scientific) was coupled to a 3000 Ultimate HPLC instrument (Thermo Fisher Scientific). The MS resolution is 60,000 at *m/z* 400; MS scan range is 300 to 1,600 *m/z*; automatic gain control target for MS and MS/MS scans are 10e6 and 5,000 respectively; isolation window is 2.0 Da; dynamic exclusion is 18 s; and collision-induced dissociation was performed on the top 15 most abundant precursor ions.

LC/MS/MS Data Analysis. LC/MS/MS data were processed with Mascot Distiller (Matrix Science). Processed peak lists were searched against the Sprot Mouse database with a decoy database using Mascot Daemon 2.5.0 (Matrix Science). The error tolerances for precursor and product ions were set at ±5 ppm and ±0.3 Da, respectively. Methionine oxidation was included as a variable modification. Peptides matched were filtered at 1% false discovery rate. The "Mascot Score" shown in *SI Appendix*, Table S1 is the Mascot protein score obtained by using the Mascot search engine for the database search. Mascot uses probability-based scoring, in which the score is the probability (P) that the observed match is a random event (www.matrixscience.com/help/scoring_help.html). Mascot scores are reported as −10Log10(P). An ion score of 100 means that for the peptide sequence matched, the chance of being a random match is 10^{-10}. The protein score is the sum of the highest ions score for each distinct sequence matched to that protein. The score varies as the database searching parameters changes. For the data shown in *SI Appendix*, Table S1, a protein with a score higher than 70 often has at least two different peptides matched to that protein.

HEK293T Maintenance and Cell Transfection. HEK293T cells were grown and maintained with 5% FBS and 1% penicillin–streptomycin in DMEM containing high glucose. For transfection, polyethyleneimine (PEI) solution (1 mg/mL in ultrapure water) was used with various cDNAs of STEP, GluA1, and GluA2. Each plasmid DNA was diluted in Opti-MEM I, to which PEI solution diluted in Opti-MEM I was added and mixed thoroughly. After 15 min of incubation at room temperature, HEK293T cells were added to the mixture and incubated for a day after transfection.

WT and STEP-KO Mouse Brain Subcellular Fractionation. The National Institute of Neurological Disorders and Stroke Animal Care and Use Committee approved our use of experimental animals (protocol #1171). All animals were handled and the experiments were performed according to these guidelines. Brain subcellular fractionation was carried out following standard methods as previously described (28). Briefly, forebrain from WT or STEP-KO mice was homogenized in ice-cold Tris buffer (320 mM sucrose, 10 mM Tris·HCl at pH 7.5, 5 mM EDTA, and protease and phosphatase inhibitor mixtures). Homogenates (H) were centrifuged to 1,000 × *g* for 10 min at 4 °C to remove nuclei and large debris. The supernatant was centrifuged to 10,000 × *g* for 15 min at 4 °C to obtain the P2 fraction. The P2 pellet was resuspended and incubated in ice-cold TEVP buffer (35.6 mM sucrose, 10 mM Tris·HCl at pH 7.5, 5 mM EDTA, and protease and phosphatase inhibitor mixtures), and then centrifuged to 25,000 × *g* for 20 min at 4 °C to obtain synaptic plasma membranes (SPM). The SPM pellet was added with 1% Triton X-100 lysis

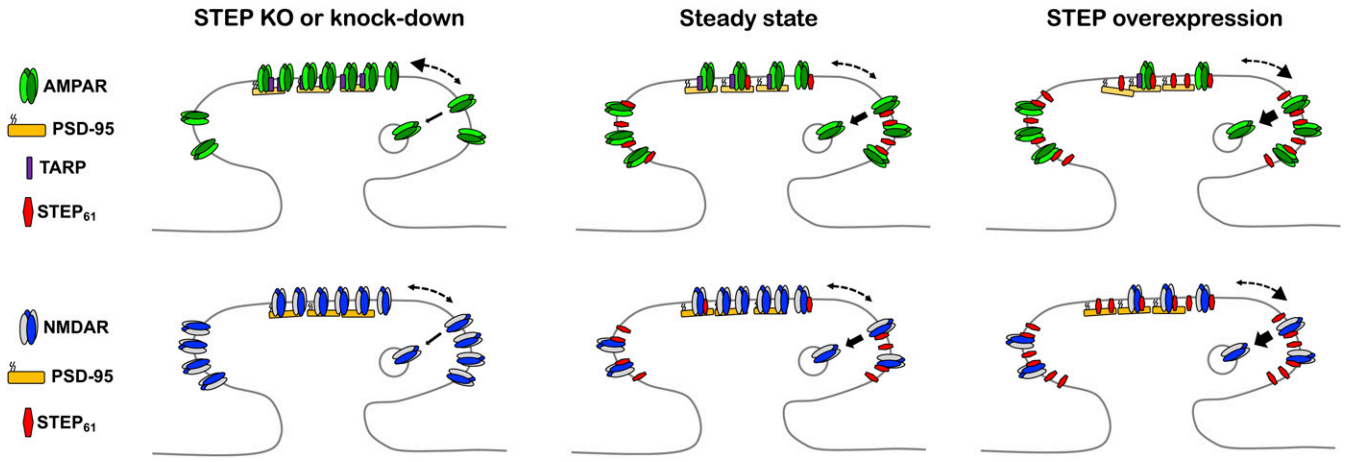

Fig. 7. Model of $STEP_{61}$ differentially regulating synaptic vs. extrasynaptic AMPA and NMDA receptors. PSD-95 acts to stabilize glutamate receptors at the PSD by directly interacting with NMDARs or by the association with AMPARs via transmembrane AMPAR regulatory proteins (TARPs). Tyrosine dephosphorylation of AMPARs or NMDARs by $STEP_{61}$ facilitates endocytosis at extrasynaptic endocytic zones. The arrow width reflects the amount of AMPAR and NMDAR trafficking. The drawing is not scaled.

buffer (1% Triton X-100, 10 mM Tris·HCl at pH 7.5, 5 mM EDTA, and protease and phosphatase inhibitor mixtures), resuspended, and incubated with gentle agitation for 30 min at 4 °C. Lysates were centrifuged to 33,000 × *g* for 30 min at 4 °C to obtain a soluble fraction and a pellet (PSD fraction), which was solubilized in 1% SDS lysis buffer (1% SDS, 10 mM Tris·HCl at pH 7.5, 5 mM EDTA, and protease and phosphatase inhibitor mixtures) for 30 min at 37 °C. Lysates were centrifuged to 100,000 × *g* for 30 min at 4 °C to obtain the PSD fraction.

Sample Preparation for MS and Coimmunoprecipitation and for GST Pull-Down Assays. For MS sample preparation and co-IP experiments, adult mouse hippocampus and cultured cortical neurons at DIV 28 were lysed with 1% sodium deoxycholate lysis buffer and then neutralized with 1% Triton X-100 lysis buffer (1% Triton X-100, 50 mM Tris·HCl at pH 7.4, 150 mM NaCl, 1 mM EDTA, and protease and phosphatase inhibitor mixtures). Lysates were incubated with anti-STEP or GluA2 antibodies overnight at 4 °C and, the next day, incubated with protein G- or A-Sepharose beads for 4 h at 4 °C, and then washed three times with 1% Triton X-100 lysis buffer and immunoblotted. For GST pull-down assays, HEK293T cells were transfected with HA- or myc-$STEP_{61}$ and lysed with 1% Triton X-100 lysis buffer. Lysates were incubated with GST-GluA1–3 C termini for 2 h at 4 °C. After three washes, bound proteins were eluted and immunoblotted for HA or myc to confirm the protein interaction.

Lentiviral Particle Packaging. To express $STEP_{61}$ in cultured cortical neurons, HEK293T cells in UltraCulture medium (cat. no. 23-725F; Lonza) containing 2 mM L-glutamine, 1 mM sodium pyruvate, 0.075% sodium bicarbonate, and 5 mM Hepes in a multilayer flask (cat. no. 1482695; Fisher Scientific) were transfected with the lentiviral vector FHUGW containing $STEP_{61}$, the packaging vector Δ8.9, and the envelope glycoprotein vector (vesicular stomatitis virus glycoprotein) by using PEI transfection solution. Two days after transfection, lentiviral particles were produced and culture medium containing lentiviral particles was collected and centrifuged at 18,000 × *g* for 3 h at 4 °C, and the lentiviral pellet was resuspended with 500 μL of PBS, aliquoted, and frozen at −80 °C.

Immunochemistry. Hippocampal neurons in 12-well plates were transduced with pCAG-IRES-mCherry and pCAG-$STEP_{61}$-IRES-mCherry at DIV 10. After 9 d, neurons were treated with chloroquine (50 μM) and MG-132 (1 μM) for 18 h and then used for immunostaining. After washing the neurons with PBS, the cells were fixed with 4% paraformaldehyde/4% sucrose in PBS for 15 min. After permeabilization with 0.25% Triton X-100 in PBS for 10 min, cells were blocked in 10% normal goat serum. To label GluA2 and PSD-95 proteins, primary antibodies were incubated overnight at 4 °C. The next day, each primary antibody was labeled with Alexa Fluor 488- or 555-conjugated secondary antibodies. Images were acquired on a Zeiss LSM 510 confocal microscope. Serial optical sections collected at 0.30-μm intervals were used to create maximum projection images. ImageJ (JACoP) was used to measure the colocalization (Mander's coefficient) of GluA2 overlapping to PSD-95 in three sections of dendrites selected and averaged for each neuron. Ten neurons were analyzed per experiment, and experiments were repeated three times independently.

Electrophysiology in Slice Cultures. Organotypic hippocampal slice cultures were made, and slices from postnatal day 6 (P6) to P8 rats were biolistically transfected at DIV 1. Recordings were performed at DIV 7 to 8. For the overexpression experiments, slices were transfected at DIV 7, and recordings made at DIV 9. Dual whole-cell recordings in area CA1 were done by simultaneously recording responses from the fluorescent transfected neuron and the neighboring untransfected control neuron. Pyramidal neurons were identified by morphology and location. Series resistance was constantly monitored, and recordings in which series increased >30 Mohm or varied by >50% between neurons were discarded. Whole-cell AMPAR and NMDAR recordings used an extracellular solution bubbled with 95% O_2/5% CO_2 consisting of 119 mM NaCl, 2.5 mM KCl, 4 mM $CaCl_2$, 4 mM $MgSO_4$, 1 mM NaH_2PO_4, 26.2 mM $NaHCO_3$, and 11 mM glucose. A 100-μM concentration of picrotoxin was added to block inhibitory currents, and 2 μM 2-chloroadenosine was used to control epileptiform activity. A bipolar stimulation electrode (Microprobe) was placed in striatum radiatum, and responses were evoked at 0.2 Hz. AMPAR currents were measured at −70 mV; NMDAR currents were measured at +40 mV and temporally isolated by measuring amplitudes 100 ms after the stimulus. Whole-cell AMPA responses were evoked at −70 mV by 1 mM glutamate delivered to the neuronal soma by a large-diameter (20- to 30-μm tip diameter) pipette, in the presence of 50 μM NMDAR antagonist D-APV (Alomone Labs). Whole-cell NMDA responses were evoked at +40 mV by 200 μM NMDA/200 μM glycine delivered to the neuronal soma by a large-diameter (20- to 30-μm tip diameter) pipette. Perfusion was 1 s in duration and was controlled by a Picospritzer II (General Valve Corp.). To block evoked potentials, 1 μM tetrodotoxin was added. Intracellular solution contained 135 mM $CsMeSO_4$, 8 mM NaCl, 10 mM Hepes, 0.3 mM EGTA, 5 mM QX314-Cl, 4 mM MgATP, 0.3 mM Na_3GTP, and 0.1 mM spermine. Data were gathered through a MultiClamp 700B amplifier (Axon Instruments), filtered at 2 kHz and digitized at 10 kHz. All data were collected through customized Igor Pro software and processed and analyzed using Microsoft Excel and Prism GraphPad 5.

Statistical Analysis. Significance of evoked dual whole-cell recordings compared with controls was determined using the Wilcoxon signed-rank sum test. Paired-pulse ratio significance was determined using the Mann–Whitney *U* test. Band densities of Western blots were measured using ImageJ software, and the statistical significance between samples was calculated using Student's *t* test (n = number of independent experiments). Statistical significance for imaging data was determined using Dunnett's one-way ANOVA test, and was considered significant at $P < 0.05$.

ACKNOWLEDGMENTS. We thank John D. Badger II and National Institute of Neurological Disorders and Stroke (NINDS) imaging facility for technical assistance, and Dr. Uimook Choi for lentivirus production. This research was supported by the NIH NINDS Intramural Research Program (S.W., Y.L., and K.W.R.) and the NIH National Institute of Mental Health Grant R01MH070957-11A1 (to S.I. and R.A.N.).

1. Lüscher C, Nicoll RA, Malenka RC, Muller D (2000) Synaptic plasticity and dynamic modulation of the postsynaptic membrane. *Nat Neurosci* 3:545–550.
2. Bredt DS, Nicoll RA (2003) AMPA receptor trafficking at excitatory synapses. *Neuron* 40:361–379.
3. Collingridge GL, Isaac JT, Wang YT (2004) Receptor trafficking and synaptic plasticity. *Nat Rev Neurosci* 5:952–962.
4. Paoletti P, Bellone C, Zhou Q (2013) NMDA receptor subunit diversity: Impact on receptor properties, synaptic plasticity and disease. *Nat Rev Neurosci* 14:383–400.
5. Henley JM, Wilkinson KA (2016) Synaptic AMPA receptor composition in development, plasticity and disease. *Nat Rev Neurosci* 17:337–350.
6. Bliss TV, Collingridge GL (1993) A synaptic model of memory: Long-term potentiation in the hippocampus. *Nature* 361:31–39.
7. Lau CG, Zukin RS (2007) NMDA receptor trafficking in synaptic plasticity and neuropsychiatric disorders. *Nat Rev Neurosci* 8:413–426.
8. Iacobucci GJ, Popescu GK (2017) NMDA receptors: Linking physiological output to biophysical operation. *Nat Rev Neurosci* 18:236–249.
9. Jacobi E, von Engelhardt J (2017) Diversity in AMPA receptor complexes in the brain. *Curr Opin Neurobiol* 45:32–38.
10. Kerchner GA, Nicoll RA (2008) Silent synapses and the emergence of a postsynaptic mechanism for LTP. *Nat Rev Neurosci* 9:813–825.
11. Lisman J, Yasuda R, Raghavachari S (2012) Mechanisms of CaMKII action in long-term potentiation. *Nat Rev Neurosci* 13:169–182.
12. Nicoll RA, Roche KW (2013) Long-term potentiation: Peeling the onion. *Neuropharmacology* 74:18–22.
13. Chater TE, Goda Y (2014) The role of AMPA receptors in postsynaptic mechanisms of synaptic plasticity. *Front Cell Neurosci* 8:401.
14. Roth RH, Zhang Y, Huganir RL (2017) Dynamic imaging of AMPA receptor trafficking in vitro and in vivo. *Curr Opin Neurobiol* 45:51–58.
15. Widagdo J, Guntupalli S, Jang SE, Anggono V (2017) Regulation of AMPA receptor trafficking by protein ubiquitination. *Front Mol Neurosci* 10:347.
16. Lussier MP, Sanz-Clemente A, Roche KW (2015) Dynamic regulation of N-Methyl-d-aspartate (NMDA) and α-Amino-3-hydroxy-5-methyl-4-isoxazolepropionic acid (AMPA) receptors by posttranslational modifications. *J Biol Chem* 290:28596–28603.
17. Shi S, Hayashi Y, Esteban JA, Malinow R (2001) Subunit-specific rules governing AMPA receptor trafficking to synapses in hippocampal pyramidal neurons. *Cell* 105:331–343.
18. Barria A, Malinow R (2002) Subunit-specific NMDA receptor trafficking to synapses. *Neuron* 35:345–353.
19. Furukawa H, Singh SK, Mancusso R, Gouaux E (2005) Subunit arrangement and function in NMDA receptors. *Nature* 438:185–192.
20. Chung HJ, Huang YH, Lau LF, Huganir RL (2004) Regulation of the NMDA receptor complex and trafficking by activity-dependent phosphorylation of the NR2B subunit PDZ ligand. *J Neurosci* 24:10248–10259.
21. Sanz-Clemente A, Nicoll RA, Roche KW (2013) Diversity in NMDA receptor composition: Many regulators, many consequences. *Neuroscientist* 19:62–75.
22. Nakazawa T, et al. (2001) Characterization of Fyn-mediated tyrosine phosphorylation sites on GluR epsilon 2 (NR2B) subunit of the N-methyl-D-aspartate receptor. *J Biol Chem* 276:693–699.
23. Sanz-Clemente A, Matta JA, Isaac JT, Roche KW (2010) Casein kinase 2 regulates the NR2 subunit composition of synaptic NMDA receptors. *Neuron* 67:984–996.
24. Lombroso PJ, Murdoch G, Lerner M (1991) Molecular characterization of a protein-tyrosine-phosphatase enriched in striatum. *Proc Natl Acad Sci USA* 88:7242–7246.
25. Lombroso PJ, Naegele JR, Sharma E, Lerner M (1993) A protein tyrosine phosphatase expressed within dopaminoceptive neurons of the basal ganglia and related structures. *J Neurosci* 13:3064–3074.
26. Bult A, et al. (1997) STEP: A family of brain-enriched PTPs. Alternative splicing produces transmembrane, cytosolic and truncated isoforms. *Eur J Cell Biol* 72:337–344.
27. Pelkey KA, et al. (2002) Tyrosine phosphatase STEP is a tonic brake on induction of long-term potentiation. *Neuron* 34:127–138.
28. Won S, Incontro S, Nicoll RA, Roche KW (2016) PSD-95 stabilizes NMDA receptors by inducing the degradation of STEP61. *Proc Natl Acad Sci USA* 113:E4736–E4744.
29. Goebel-Goody SM, et al. (2012) Therapeutic implications for striatal-enriched protein tyrosine phosphatase (STEP) in neuropsychiatric disorders. *Pharmacol Rev* 64:65–87.
30. Zhang Y, et al. (2010) Genetic reduction of striatal-enriched tyrosine phosphatase (STEP) reverses cognitive and cellular deficits in an Alzheimer's disease mouse model. *Proc Natl Acad Sci USA* 107:19014–19019.
31. Carty NC, et al. (2012) The tyrosine phosphatase STEP: Implications in schizophrenia and the molecular mechanism underlying antipsychotic medications. *Transl Psychiatry* 2:e137.
32. Darnell JC, et al. (2011) FMRP stalls ribosomal translocation on mRNAs linked to synaptic function and autism. *Cell* 146:247–261.
33. Saavedra A, et al. (2011) Striatal-enriched protein tyrosine phosphatase expression and activity in Huntington's disease: A STEP in the resistance to excitotoxicity. *J Neurosci* 31:8150–8162.
34. Braithwaite SP, et al. (2008) Expression and function of striatal enriched protein tyrosine phosphatase is profoundly altered in cerebral ischemia. *Eur J Neurosci* 27: 2444–2452.
35. Nguyen TH, Liu J, Lombroso PJ (2002) Striatal enriched phosphatase 61 dephosphorylates Fyn at phosphotyrosine 420. *J Biol Chem* 277:24274–24279.
36. Blanco-Aparicio C, Torres J, Pulido R (1999) A novel regulatory mechanism of MAP kinases activation and nuclear translocation mediated by PKA and the PTP-SL tyrosine phosphatase. *J Cell Biol* 147:1129–1136.
37. Paul S, Nairn AC, Wang P, Lombroso PJ (2003) NMDA-mediated activation of the tyrosine phosphatase STEP regulates the duration of ERK signaling. *Nat Neurosci* 6: 34–42.
38. Xu J, et al. (2012) Striatal-enriched protein-tyrosine phosphatase (STEP) regulates Pyk2 kinase activity. *J Biol Chem* 287:20942–20956.
39. Roche KW, et al. (2001) Molecular determinants of NMDA receptor internalization. *Nat Neurosci* 4:794–802.
40. Lavezzari G, McCallum J, Lee R, Roche KW (2003) Differential binding of the AP-2 adaptor complex and PSD-95 to the C-terminus of the NMDA receptor subunit NR2B regulates surface expression. *Neuropharmacology* 45:729–737.
41. Lavezzari G, McCallum J, Dewey CM, Roche KW (2004) Subunit-specific regulation of NMDA receptor endocytosis. *J Neurosci* 24:6383–6391.
42. Zhang Y, et al. (2008) The tyrosine phosphatase STEP mediates AMPA receptor endocytosis after metabotropic glutamate receptor stimulation. *J Neurosci* 28: 10561–10566.
43. Kurup P, et al. (2010) Abeta-mediated NMDA receptor endocytosis in Alzheimer's disease involves ubiquitination of the tyrosine phosphatase STEP61. *J Neurosci* 30: 5948–5957.
44. Hayashi T, Huganir RL (2004) Tyrosine phosphorylation and regulation of the AMPA receptor by SRC family tyrosine kinases. *J Neurosci* 24:6152–6160.
45. Muñoz JJ, Tárrega C, Blanco-Aparicio C, Pulido R (2003) Differential interaction of the tyrosine phosphatases PTP-SL, STEP and HePTP with the mitogen-activated protein kinases ERK1/2 and p38alpha is determined by a kinase specificity sequence and influenced by reducing agents. *Biochem J* 372:193–201.
46. Gladding CM, et al. (2012) Calpain and STriatal-enriched protein tyrosine phosphatase (STEP) activation contribute to extrasynaptic NMDA receptor localization in a Huntington's disease mouse model. *Hum Mol Genet* 21:3739–3752.
47. Snyder EM, et al. (2005) Regulation of NMDA receptor trafficking by amyloid-beta. *Nat Neurosci* 8:1051–1058.
48. Jang SS, et al. (2015) Regulation of STEP61 and tyrosine-phosphorylation of NMDA and AMPA receptors during homeostatic synaptic plasticity. *Mol Brain* 8:55.
49. Lu W, et al. (2009) Subunit composition of synaptic AMPA receptors revealed by a single-cell genetic approach. *Neuron* 62:254–268.
50. Gainey MA, Hurvitz-Wolff JR, Lambo ME, Turrigiano GG (2009) Synaptic scaling requires the GluR2 subunit of the AMPA receptor. *J Neurosci* 29:6479–6489.
51. Boulanger LM, et al. (1995) Cellular and molecular characterization of a brain-enriched protein tyrosine phosphatase. *J Neurosci* 15:1532–1544.
52. Bult A, et al. (1996) STEP61: A member of a family of brain-enriched PTPs is localized to the endoplasmic reticulum. *J Neurosci* 16:7821–7831.
53. Paul S, et al. (2007) The striatal-enriched protein tyrosine phosphatase gates long-term potentiation and fear memory in the lateral amygdala. *Biol Psychiatry* 61: 1049–1061.
54. Xu J, et al. (2009) Extrasynaptic NMDA receptors couple preferentially to excitotoxicity via calpain-mediated cleavage of STEP. *J Neurosci* 29:9330–9343.
55. Lussier MP, et al. (2012) Ubiquitin ligase RNF167 regulates AMPA receptor-mediated synaptic transmission. *Proc Natl Acad Sci USA* 109:19426–19431.